
Layer-level activation mechanism

Kihyuk Yoon

Department of Industrial Engineering
UNIST

Chiehyeon Lim

Department of Industrial Engineering
UNIST

Abstract

In this work, we propose a novel activation mechanism aimed at establishing layer-level activation (LayerAct) functions. These functions are designed to be more noise-robust compared to traditional element-level activation functions by reducing the layer-level fluctuation of the activation outputs due to shift in inputs. Moreover, the LayerAct functions achieve a zero-like mean activation output without restricting the activation output space. We present an analysis and experiments demonstrating that LayerAct functions exhibit superior noise-robustness compared to element-level activation functions, and empirically show that these functions have a zero-like mean activation. Experimental results on three benchmark image classification tasks show that LayerAct functions excel in handling noisy image datasets, outperforming element-level activation functions, while the performance on clean datasets is also superior in most cases.

1 Introduction

Various activation functions have been proposed to enhance the effectiveness and efficiency of neural networks training. Previous studies have identified significant properties of activation functions: i) one-sided saturation (e.g., rectified linear unit (ReLU [7, 20]) that saturates only negative side of outputs) to avoid the vanishing gradient problem while maintaining noise-robustness, and ii) allowing negative output for a zero-like mean of activation (see Appendix A for mathematical definition of zero-like mean activation) for effective and efficient training [4, 22]. Modern activation functions, such as exponential linear unit (ELU [4]), flexible ReLU (FReLU, [4, 22]), and sigmoid-weighted linear unit (SiLU, also known as Swish, [5, 23]), seek a balance between the properties. They only saturate the large negative outputs for noise-robustness, while allowing the activation functions to produce small negative outputs for zero-like mean activation.

Nevertheless, existing activation functions that operate on a single element of the activation input (i.e., a unit of a layer) exhibit two limitations underlying their element-level activation mechanisms. Firstly, there is a trade-off between two properties of element-level activation, one-sided saturation (limiting negative output space) and allowing negative outputs. One-sided saturation naturally restricts the negative space of the activation outputs, leading the mean of activation outputs to be far from zero. This trade-off is apparent not only in ReLU, which never permits negative outputs, but also in the activation functions like ELU or FReLU that allow small negative outputs. Secondly, the noise-robustness varies across samples. The noise-robustness of element-level activation functions relies only on saturation state. This implies that existing activation functions can ensure noise-robustness for samples only when a sufficiently large number of elements are in the saturation state, not when there are fewer elements in the saturation state.

To address these issues with element-level activation functions, we propose a novel activation mechanism and two LayerAct functions, denoted as LA-SiLU and LA-HardSiLU. The trade-off problem of element-level activation functions arises because the activation input space that leads activation outputs to be in saturation state remains fixed across all samples. Unlike the element-level activation mechanism, our proposed layer-level activation mechanism assigns the saturation state

based on the normalized input of the layer-dimension, similar to layer normalization (LayerNorm; [1]). As a result, the activation output space of the saturation state varies between samples; the activation input space leading to saturation state is determined by the layer-dimension mean and variance. Furthermore, the noise-robustness of LayerAct functions does not fully depend on the number of the elements in the saturation state. We demonstrate that the upper bound of activation fluctuation due to shift of layer input can be lower with LayerAct functions than with element-level activation functions.

Experimental analysis with the MNIST image dataset revealed the following properties of the LayerAct functions: i) the mean activation of LayerAct functions is zero-like, and ii) the output fluctuation due to noisy input is smaller with these functions than that with element-level activation functions. Additionally, we compared the performance of the LayerAct functions with other element-level activation functions on three image classification tasks. The results on noisy CIFAR10 and CIFAR100 datasets demonstrate that LayerAct functions were superior to other element-level activation functions. Furthermore, ResNet50 with LayerAct functions also showed superior performance on both clean and noisy ImageNet datasets compared to other functions.

2 Background

2.1 Activation scale

Consider a layer in a multi-layer perceptron with linear projection and an activation function. The computation of this layer, given a r -dimensional input vector $x = (x_1, x_2, \dots, x_r)^T$, a weight matrix $W \in \mathbb{R}^{r \times d}$, and non-linear activation function f is defined as follows:

$$y = W^T x, \quad a = f(y), \quad (1)$$

where $y = (y_1, y_2, \dots, y_d)^T$ and a are the d -dimensional output vectors of the linear projection and activation of a layer, respectively. The output vector y of the linear projection and activation vector a serves as the input of the activation function and the input of the next layer, respectively.

In some activation functions, a function bounded between one and zero characterizes the non-linearity of the activation function during forward-propagation. We define this function, denoted as s , and its output as the *activation scale function* and *activation scale*, respectively. The activation output during forward pass and gradient during backward pass of an element-level activation functions with activation scale function s are:

$$a_i = y_i s(y_i), \quad \frac{\partial a_i}{\partial y_i} = s(y_i) + y_i \frac{\partial s(y_i)}{\partial y_i}, \quad (2)$$

where s is increasing and $s(y_i) > 0$ if $y_i > 0$. For example, the activation scale functions for the i^{th} element in ReLU and SiLU, are presented as follows:

$$s^{ReLU}(y_i) = \begin{cases} 1, & \text{if } y_i \geq 0 \\ 0, & \text{if } y_i < 0 \end{cases}, \quad s^{SiLU}(y_i) = \frac{1}{1 + e^{-y_i}} \quad (3)$$

where y_i , *sigmoid*, s^{ReLU} , and s^{SiLU} , present the i^{th} element of y , Logistic Sigmoid function, and the non-linear scale functions of ReLU and SiLU, respectively.

Furthermore, the saturation state of such activation functions can be defined using the activation scale:

Definition 2.1 (Saturation state of activation functions with activation scale functions). *The saturation state of an activation function with an activation scale function s is when $s(y_i) \simeq 0$, as the activation output $a_i = y_i s(y_i)$ reaches saturation.*

In conclusion, the activation scale function plays a crucial role in providing non-linearity during the forward pass, controlling the gradient during the backward pass, and determining the saturation state of the activation function.

2.2 Trade-off between saturation and zero-like mean activation

Element-level activation functions that exhibit saturation, such as ReLU, are well recognized for their noise-robustness properties, for instance, samples with a large number of elements in the saturation

state are noise-robust [4, 22]). However, the saturation in these functions does not allow negative outputs, which causes the mean of the activation outputs to be far from zero, potentially leading to inefficient training [4].

To address this issue, recent activation functions, such as ELU, FReLU, and SiLU, saturate only the large negative outputs. These activation functions can achieve a zero-like mean activation with small negative outputs. However, a trade-off still exists because the restriction of negative outputs, designed to ensure saturation, prevents the allowance of large negative outputs, thereby restraining the mean of activation from being more zero-like. Additionally, saturation that relies solely on the input of a single element can result a large variance in noise-robustness between samples.

2.3 Large variance of noise-robustness across samples

To analyze the noise-robustness, we define activation fluctuation (i.e., fluctuation of activation outputs due to the shift of inputs) that can represent the layer-level noise-robustness on a sample.

Definition 2.2 (Activation fluctuation). *Let $\epsilon = (\epsilon_1, \epsilon_2, \dots, \epsilon_d)^T$ be the noise vector. We define activation fluctuation as $\|f(y + \epsilon) - f(y)\| \leq c$, where c is the upper bound of activation fluctuation.*

The lower the upper bound c is, the lower the variance of noise-robustness across samples. We can define the activation fluctuation of element-level activation functions:

Definition 2.3 (Activation fluctuation of element-level activation functions). *Let ϵ_i be the i^{th} noise, and $\hat{y}_i = y_i + \epsilon_i$. The activation fluctuation of element-level activation function f is given by:*

$$\|f(\hat{y}) - f(y)\| = \sum_{i=1}^d |\hat{y}_i s(\hat{y}_i) - y_i s(y_i)| = \sum_{i=1}^d |y_i (s(\hat{y}_i) - s(y_i)) + \epsilon_i s(\hat{y}_i)|,$$

A sample will exhibit a small $\|f(\hat{y}) - f(y)\|$ if a sufficient number of its elements are in saturation state. However, element-level activation functions do not ensure that all samples have a sufficient number of elements in saturation state. More specifically, the activation fluctuation is upper-bounded when not all elements are in the saturation state, where $y_i > 0$ for all i :

$$\|f(\hat{y}) - f(y)\| \leq \sum_{i=1}^d (y_i |s(\hat{y}_i) - s(y_i)| + |\epsilon_i| \cdot s(\hat{y}_i)) \quad (4)$$

Equation 4 demonstrates that activation scale is closely related to the activation fluctuation, samples with large $\|s(\hat{y}) - s(y)\|$ and $\|s(\hat{y})\|$ are not robust to noise. Thus, a method that can reduce the upper bound of $\|s(\hat{*}) - s(*)\|$ and $\|s(\hat{*})\|$ will reduce the upper bound of activation fluctuation, resulting in a low variance of noise-robustness across samples.

2.4 Layer Normalization

LayerNorm normalizes elements along the layer-dimension, as opposed to the batch-dimension in batch normalization (BatchNorm, [11]). LayerNorm normalizes the elements of a layer using the layer-dimension mean μ_y and standard deviation σ_y defined as follows:

$$n_i^{LN} = \frac{g_i}{\sigma_y} (y_i - \mu_y) + b_i, \quad \mu_y = \frac{1}{d} \sum_{i=1}^d y_i, \quad \sigma_y = \sqrt{\frac{1}{d} \sum_{i=1}^d (y_i - \mu_y)^2} \quad (5)$$

where n_i^{LN} , g_i , and b_i are the i^{th} normalized output, gain, and bias of LayerNorm. With LayerNorm, the sum of activation scale $\|s(n^{LN})\|$ will be similar across all samples, which helps to reduce the variance of noise-robustness across all samples. However, LayerNorm loses all the mean and variance statistics of linear projection y ; thus, the final outputs of the layer across samples become similar [14, 17]. To avoid this dilution problem, a layer-level balancing mechanism should be employed that does not directly re-scale or re-center the activation input.

In this section, we have defined activation scale function and demonstrated its critical role in activation processes: 1) provides non-linearity during forward pass, 2) controls gradient during backward pass, and 3) is related to the noise-robustness of the model. We demonstrated that element-level activation functions may have large variance of noise-robustness across samples. LayerNorm can reduce such variance of the noise-robustness by re-scaling and re-centering the activation input, but it also causes the statistics of activation outputs to be similar across all samples.

3 Layer-level activation

In this section, we introduce and discuss a novel layer-level activation mechanism and associated functions that utilize layer-dimension normalized input for the activation scale function (see Figure 1). Our proposed method does not suffer from the trade-off issue and exhibits lower variance than element-level activation functions across samples. Importantly, it does not cause the dilution problem that statistics of activation outputs to become similar.

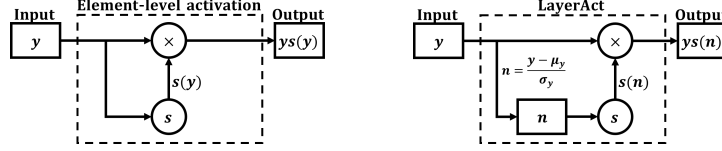


Figure 1: The mechanisms of the element-level activation (left) and proposed layer-level activation (right).

3.1 LayerAct mechanism

The LayerAct function is defined as the product of the input y_i and the activation scale $s(n_i)$ which uses the layer-normalized input n_i . The forward pass of a LayerAct function is given by:

$$a_i = y_i s(n_i), \quad n_i = \frac{(y_i - \mu_y)}{\sqrt{\sigma_y^2 + \alpha}} \quad (6)$$

where $\alpha > 0$ is a constant that introduced for stability, μ_y , and σ_y are the layer-dimension mean and standard deviation, respectively. Using the chain rule, the backward pass can be described as follows:

$$\begin{aligned} \frac{\partial \mathcal{L}}{\partial \mu} &= \sum_{i=1}^d \frac{\partial \mathcal{L}}{\partial a_i} \cdot \frac{\partial s(n_i)}{\partial n_i} \cdot \frac{-y_i}{\sqrt{\sigma^2 + \alpha}}, \\ \frac{\partial \mathcal{L}}{\partial \sigma^2} &= \sum_{i=1}^d \frac{\partial \mathcal{L}}{\partial a_i} \cdot \frac{\partial s(n_i)}{\partial n_i} \cdot \frac{-y_i \cdot n_i}{2(\sigma^2 + \alpha)}, \\ \frac{\partial \mathcal{L}}{\partial y_i} &= \frac{\partial \mathcal{L}}{\partial a_i} s(n_i) + \frac{\partial \mathcal{L}}{\partial a_i} \cdot \frac{\partial s(n_i)}{\partial n_i} \cdot \frac{y_i}{\sqrt{\sigma^2 + \alpha}} \\ &\quad + \frac{1}{d} \cdot \frac{\partial \mathcal{L}}{\partial \mu} + \frac{2(y_i - \mu)}{d} \cdot \frac{\partial \mathcal{L}}{\partial \sigma^2}. \end{aligned}$$

Notably, the activation output a_i in Equation 6 is not normalized output of activation input y . Unlike activation with LayerNorm, which results in the activation output $a_i = n_i s(n_i)$ and erases all mean and variance statistics from the input vector, the LayerAct functions can deliver the mean and variance of input to output. For the detail on difference between LayerAct and activation with LayerNorm, see Appendix B.

For stable learning and inference, it is crucial for the activation outputs to remain continuous throughout the entire output space. While element-level activation functions such as ReLU, leaky ReLU (LReLU [18]), and parametric ReLU (PReLU, [8]) do not require the activation scale to be continuous at zero (since the activation output $y_i s(y_i)$ is still continuous at zero), this is not the case for LayerAct functions, where the activation output $y_i s(n_i)$ is discontinuous if the activation scale function is not continuous. Hence, we define specific activation scale function s for LayerAct mechanism:

Definition 3.1 (Activation scale function for LayerAct functions). *The activation scale function s is an increasing Lipschitz continuous function that bounded between zero and one:*

$$s(0) = 1/2, \quad |s(a) - s(b)| \leq K |a - b| \quad \forall a, b \in \mathbb{R}.$$

Any function that satisfies Definition 3.1 can be used as an activation scale function for a LayerAct function. In this paper, we suggest the Sigmoid and HardSigmoid functions as simple activation scale functions for LayerAct functions. Both the functions are Lipschitz continuous functions and bounded between 0 and 1. We propose the following two LayerAct functions, LA-SiLU and LA-HardSiLU, which are the layer-level transformed versions of SiLU and HardSiLU, respectively:

$$LA-SiLU(y_i) = \frac{y_i}{1 + e^{-n_i}}, \quad LA-HardSiLU(y_i) = \begin{cases} y_i, & \text{if } n_i \geq 3 \\ y_i \left(\frac{n_i}{6} + \frac{1}{2}\right), & \text{if } -3 \leq n_i < 3 \\ 0, & \text{if } n_i < -3 \end{cases}.$$

3.2 Properties of LayerAct

No trade-off between saturation and negative outputs. LayerAct, unlike element-level activations, bypasses the trade-off between saturation and zero-like mean activation. The key distinction in saturation between the element-level and LayerAct functions is that saturation state of element-level functions requires to be fixed at a certain point of activation output, whereas that of LayerAct functions depends on layer-dimension normalized inputs. Thus, while LayerAct still have saturation state where $s(n_i) \simeq 0$, the activation output space with a LayerAct function is not limited (e.g., consider a layer where $\mu_y \ll 0$).

Relationship with normalization methods. The LayerAct functions can be used in conjunction with normalization methods that have different normalization direction, such as BatchNorm, which have been successful across various deep learning domains [2]. Conversely, the beneficial properties of LayerAct might be diminished when it is used right after LayerNorm, where the activation inputs are already normalized in layer-direction. However, this does not imply that the LayerAct functions are unsuitable for networks with LayerNorm. LayerAct functions can be employed in networks where the activation and LayerNorm do not correspond one-to-one, such as the LSTM-based models presented by Ba et al. [1]. For the detail, see Appendix C.

3.3 Noise-robustness of LayerAct

In this subsection, we begin by establishing that the activation fluctuation of LayerAct is also related to the two terms of activation scale function, $\|s(\hat{*}) - s(*)\|$ and $\|s(\hat{*})\|$, as outlined in Subsection 2.3. Subsequently, we demonstrate that these two terms for LayerAct are bound to be lower than those of element-level activation. Here, we consider noise that is not substantial compared to activation input (i.e., $\sigma_\epsilon \ll \sigma_y$), where σ_ϵ represents the variance of noise ϵ . To begin with, we define the activation fluctuation of LayerAct.

Definition 3.2 (Activation fluctuation of LayerAct functions). *The activation fluctuation of LayerAct activation function g , where $\hat{n}_i = (\hat{y}_i - \mu_{\hat{y}}) / \sigma_{\hat{y}}$ denotes i^{th} noisy normalized input, is defined as:*

$$\|g(\hat{y}) - g(y)\| = \sum_{i=1}^d |\hat{y}_i s(\hat{n}_i) - y_i s(n_i)| = \sum_{i=1}^d |y_i (s(\hat{n}_i) - s(n_i)) + \epsilon_i s(\hat{n}_i)|,$$

Given that n and \hat{n} represent the normalized output of y and \hat{y} , respectively, we can define an upper bound for the activation fluctuation of LayerAct functions as follows:

$$\|g(\hat{y}) - g(y)\| \leq \sum_{i=1}^d (|y_i| |s(\hat{n}_i) - s(n_i)| + |\epsilon_i| s(\hat{n}_i)). \quad (7)$$

Hence, the two terms of LayerAct scale function, $\|s(\hat{n}) - s(n)\|$ and $\|s(\hat{n})\|$, are also related to the noise-robustness, similar to those of element-level activation function (see Equation 4). Considering Definition 3.1, the upper bound of $\|s(\hat{y}) - s(y)\|$ and $\|s(\hat{y})\|$ of element-level activation and that of $\|s(\hat{n}) - s(n)\|$ and $\|s(\hat{n})\|$ of LayerAct are given by respectively:

$$\|s(\hat{y}) - s(y)\| \leq \sum_{i=1}^d K |\epsilon_i|, \quad \|s(\hat{y}_i)\| \leq d, \quad (8)$$

$$\|s(\hat{n}) - s(n)\| < K \sum_i^d \left| \frac{y_i + \epsilon_i - \mu_y - \mu_\epsilon}{\sqrt{\sigma_y^2 + \alpha + \sigma_\epsilon^2}} - \frac{y_i - \mu_y}{\sqrt{\sigma_y^2 + \alpha}} \right| = \sum_i^d \frac{K |\epsilon_i - \mu_\epsilon|}{\sqrt{\sigma_y^2 + \alpha}}, \quad \|s(\hat{n}_i)\| = \frac{d}{2}, \quad (9)$$

where $\sqrt{\sigma_y^2 + \alpha + \sigma_\epsilon^2} \simeq \sqrt{\sigma_y^2 + \alpha} > 1$ when $\sigma_y \gg \sigma_\epsilon$ and α is sufficiently large.

Equation 8 and 9 reveal that the activation fluctuation of LayerAct can exhibit a smaller boundary across samples compared to that of element-level activation. This suggests that LayerAct can ensure more robust processing during forward pass of a network. Moreover, the noise-robustness of the LayerAct does not fully rely on the saturation state, which can cause negative effects in training a network [26].

4 Experiment

In this section, we present the experimental analysis and classification performance of LayerAct. First, we verify the important properties of LayerAct with the MNIST dataset. Next, we evaluate the classification performance of the LayerAct functions on three image datasets, CIFAR10, CIFAR100 [12], and ImageNet [24] for both clean and noisy cases. We used ResNets as the network architecture for our experiments [9]. See Appendix E for details of the experimental environment, and Appendix G for more result of experiments.

4.1 Experimental analysis on MNIST

In this subsection, we compare the LayerAct functions with other activation functions to demonstrate that LayerAct functions embody the properties discussed in Section 3: i) zero-like mean activation and ii) noise-robustness. We trained a network with a single layer that contains 512 elements on the MNIST training dataset without any noise to observe the behavior of the LayerAct functions during training. For the detail of experimental setting, see Appendix E.

4.1.1 Zero-like mean activation

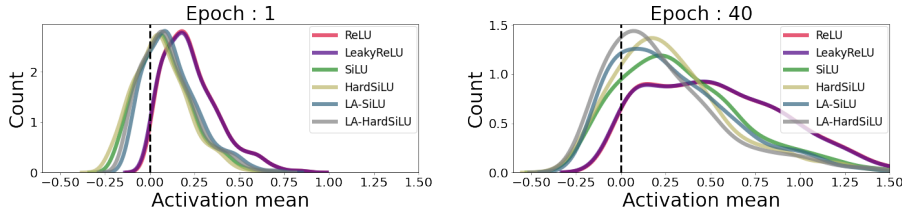


Figure 2: Distribution of the activation output means of the elements in a trained network on MNIST at 1 and 40 epochs. The distributions did not change after 40 epochs. The LayerAct functions maintain zero-like mean activation for all epochs.

Figure 2 shows the distribution of the activation output means of the single-layer network trained on the MNIST dataset. Our experimental results indicate that the LayerAct functions allow similar (before epoch 20) or larger (after epoch 40) negative outputs compared to the element-level activation functions with negative outputs. Thus, LA-SiLU and LA-HardSiLU can achieve more zero-like mean activation than other activation functions.

4.1.2 Noise-robustness

To confirm the noise-robustness of the LayerAct functions, we computed the activation fluctuation of Definition 2.3 and 3.2 using the network trained on the clean MNIST dataset. For the noisy input \hat{y}_i , we used two different noises with a normal distribution.

Figure 3 shows the distribution of the activation fluctuation with two different noise distributions. Although the fluctuation distribution of the activation input was similar (See Figure 4 in Appendix G), LayerAct functions have a significantly smaller mean and variance of activation fluctuation among the samples than any other element-level activation function in all cases. The decrease in variance is remarkable, showing that the LayerAct functions are noise-robust for all samples. Moreover, the element-level activation functions that ensure a zero-like mean with one-sided saturation such as SiLU or HardSiLU showed slightly larger activation fluctuations than those of ReLU or LReLU when

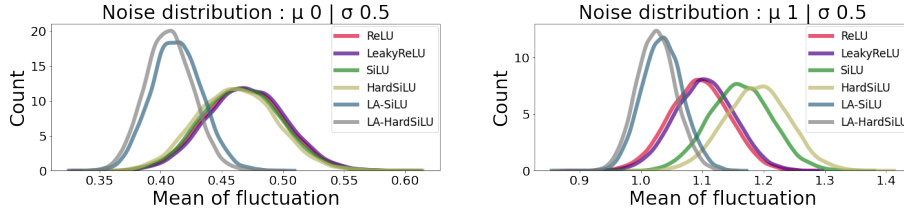


Figure 3: Distribution of activation output fluctuation due to noise with different noise distribution. The activation fluctuation of the LayerAct functions have lower mean and variance than those of the other element-level activation functions in both cases.

the noise had a large mean. However, the LayerAct functions maintained lower fluctuations in both cases.

4.2 Classification performance

We demonstrate the classification performance of the LayerAct functions on three image datasets, CIFAR10, CIFAR100, and ImageNet. We trained ResNet20, ResNet32, and ResNet44 with a basic block for CIFAR10 and CIFAR100. For ImageNet, we trained ResNet50 with the bottleneck block. In all our experiments, we utilized networks with BatchNorm. We compared the LayerAct functions with ReLU, LReLU, PReLU, Mish[19], SiLU and HardSiLU. We used accuracy as the performance metric. See Appendix E for the detail of experimental setting.

Table 1: Classification performance on the clean CIFAR10 and CIFAR100.

	CIFAR10			CIFAR100		
	ResNet20	ResNet32	ResNet44	ResNet20	ResNet32	ResNet44
ReLU	91.29	92.03	92.03	65.92	67.04	68.02
LReLU	91.31	92.03	92.03	65.88	67.37	67.96
PReLU	90.82	92.03	-	64.00	66.35	67.68
Mish	91.48	<u>92.21</u>	92.30	65.85	67.18	68.06
SiLU	91.45	92.17	92.18	65.89	67.22	67.71
HardSiLU	91.09	91.77	91.42	65.19	66.49	66.38
LA-SiLU	91.60	92.20	92.36	66.39	67.74	68.07
LA-HardSiLU	91.21	91.68	91.36	66.16	66.63	65.51

4.2.1 CIFAR10 and CIFAR100

Table 1 presents the average classification performance of both LayerAct functions and element-level activation functions over 30 runs, benchmarked on the clean CIFAR10 and CIFAR100 dataset. The best results are underlined and bolded, while the second best are bolded. One trial of Resnet44 with PReLU on CIFAR10 exploded during training. Among the element-level activation functions, networks with Mish outperformed other functions on CIFAR10, whereas ResNet20 with ReLU and ResNet32 with LReLU exhibited superior performance on CIFAR100. However, the performance of LA-SiLU was stable, showing similar or better performance than other activation functions in most cases. In statistical significance test, networks with LA-SiLU outperformed a significant majority, specifically 30 out of 36, of networks with element-level activation functions (T-test or Wilcoxon signed-rank test with p -value < 0.05).

4.2.2 Noisy CIFAR10 and CIFAR100

To verify the noise-robustness of LayerAct functions, we evaluated their classification performance on the noisy datasets, using networks that were trained on clean datasets. We selected three different types of noise which are easily found in real-world datasets: Gaussian distributed noise [25], Poisson

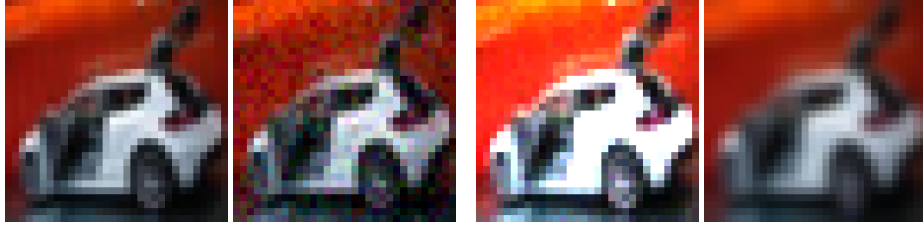


Figure 4: Clean and noisy car images of the CIFAR10 dataset. From left to right, the images are a clean image, an image with the Gaussian distributed noise, an image with Poisson distributed noise, and a Gaussian blurred image.

Table 2: Classification performance on the noisy CIFAR10.

	CIFAR10/ResNet44					
	Gaussian Noise 1	Gaussian Noise 2	Gaussian Noise 3	Gaussian Noise 4	Poisson Noise	Gaussian Blur
ReLU	69.74	68.96	29.95	30.12	73.71	57.16
LReLU	69.04	68.48	29.64	30.29	74.84	57.16
Mish	66.02	65.48	26.33	26.79	75.28	55.74
SiLU	65.93	65.25	26.19	26.61	74.32	55.04
HardSiLU	68.23	67.46	28.83	29.43	72.77	56.56
LA-SiLU	68.45	68.07	28.98	29.53	83.92	59.59
LA-HardSiLU	69.97	69.56	32.27	32.62	81.82	60.23

distributed noise [15], and Gaussian blur [6]. Specifically, we experimented with six different noisy cases: i) Gaussian distributed noise with mean and standard deviation as 0 and 0.05, ii) 0.1 and 0.05, iii) 0 and 0.1, iv) 0.1 and 0.1, v) Poisson distributed noise, and vi) Gaussian blur noise with kernel size and standard deviation as (3, 3) and 1 (See Figure 4 for the examples of noisy data). We added the noise after re-scaling the data between 0 and 1.

Table 2 and 3 shows the classification performance of ResNet44 on noisy CIFAR10 and CIFAR100 datasets as the mean accuracy over 30 runs (see Appendix G for the results of ResNet20 and ResNet32). The best results are underlined and bolded, while the second best are bolded. We do not report the experiments of ResNet44 with PReLU on CIFAR10 as a network exploded during training. On all noisy datasets, networks with LA-HardSiLU showed better performance. In statistical significance test, networks with LA-HardSiLU outperformed those with element-level activation functions (T-test or Wilcoxon signed-rank test with p -value < 0.05), except networks with ReLU and LReLU on noisy CIFAR10 with Gaussian noise 1 and 2. This result demonstrates that LA-HardSiLU exhibits greater noise-robustness to intense noise compared to other functions.

4.2.3 ImageNet

Table 4 shows the classification performance of the LayerAct functions and the element-level activation functions for comparison with clean and noisy ImageNet datasets. We report the accuracy of 10-crop testing on validation dataset. The best results are underlined and bolded, while the second best are bolded. For ImageNet, we experimented on four different noisy cases: i) Gaussian distributed noise with 0 and standard deviation 0.1, ii) Gaussian distributed noise with 0.1 and standard deviation 0.1, iii) Poisson distributed noise, and iv) Gaussian blur noise with kernel size and standard deviation as (7, 7) and 3. The networks with LayerAct functions outperformed those with other activation functions on all datasets. The LayerAct functions, even LA-HardSiLU that showed worse performance on the clean CIFAR10 and CIFAR100 datasets than SiLU or LReLU, outperformed other activation functions. We report more trials with different random seed for weight initialization in Appendix G.

Table 3: Classification performance on the noisy CIFAR100.

	CIFAR100/ResNet44					
	Gaussian Noise 1	Gaussian Noise 2	Gaussian Noise 3	Gaussian Noise 4	Poisson Noise	Gaussian Blur
ReLU	32.01	31.98	10.50	10.37	22.62	32.66
LReLU	32.14	32.31	10.77	10.78	22.97	33.32
PReLU	32.78	32.51	10.75	10.40	21.84	31.52
Mish	30.30	30.36	9.67	9.73	22.82	33.11
SiLU	30.83	30.86	10.33	10.21	20.11	32.91
HardSiLU	33.49	33.59	11.39	11.34	19.44	34.21
LA-SiLU	34.81	35.44	11.85	12.57	34.38	36.84
LA-HardSiLU	40.51	41.25	16.08	17.07	36.19	39.72

Table 4: Classification performance on the clean and noisy ImageNet.

	ImageNet/ResNet50				
	Without noise	Gaussian noise 1	Gaussian noise 2	Poisson noise	Gaussian blur
ReLU	77.71	70.73	69.03	6.55	67.91
LReLU	77.83	70.41	68.69	9.29	67.88
PReLU	74.99	64.77	63.39	8.32	63.64
Mish	77.41	69.22	67.60	14.25	67.45
SiLU	77.85	69.68	68.54	9.52	67.42
HardSiLU	76.30	67.49	65.89	24.64	65.51
LA-SiLU	78.62	71.40	70.76	43.07	69.12
LA-HardSiLU	78.23	71.81	71.23	47.36	67.91

5 Discussion

Activation functions form the backbone of neural networks. To the best of our knowledge, this study is the first to develop a layer-level activation mechanism for achieving both zero-like mean activation and noise-robustness, which are the important properties of effective activation. The theoretical and experimental analyses in this study support the potential of the LayerAct functions to develop robust deep learning frameworks with high-performance. Although we suggest only two LayerAct functions in this study, it is possible to devise other LayerAct functions with suitable activation scale functions which can ensure zero-like mean activation and noise-robustness.

In this paper, we only introduced unbounded LayerAct functions, LA-SiLU and LA-HardSiLU. Such activation functions may not be directly utilized with the RNN-based networks. For RNN-based networks, bounded activation functions (i.e., functions that saturate both negative and positive sides) such as Sigmoid or Tanh are commonly utilized [10, 3]. Therefore, the development of bounded LayerAct functions is one of our future research directions.

6 Conclusion

In this study, we introduce a novel layer-level activation mechanism and LayerAct functions. Unlike the element-level activation functions, where non-linearity is directly dependent on the input of a single element, LayerAct functions provide non-linearity with layer-direction normalized input of all elements in the layer. This unique activation mechanism enables LayerAct functions to achieve one-sided saturation while also allowing larger negative outputs. Moreover, the activation scale with normalized input enables the LayerAct functions to reduce the mean and variance of activation fluctuation, implying that networks with LayerAct functions have lower variance of noise-robustness across samples. These properties of LayerAct functions are verified through experiments on the MNIST dataset. Networks trained using LA-SiLU, one of the possible LayerAct functions, demonstrated similar or better performance than those for the other activation functions on the clean image datasets. Moreover, LA-HardSiLU outperformed the other activation functions at most of the experiments on noisy datasets.

References

- [1] BA, J. L., KIROS, J. R., AND HINTON, G. E. Layer normalization. *arXiv:1607.06450* (2016).
- [2] BJORCK, N., GOMES, C. P., SELMAN, B., AND WEINBERGER, K. Q. Understanding batch normalization. In *Preceeding of NeurIPS* (2018), vol. 31.
- [3] CHO, K., MERRIENBOER, B., GULCEHRE, C., BOUGARES, F., SCHWENK, H., AND BENGIO, Y. Learning phrase representations using rnn encoder-decoder for statistical machine translation. In *EMNLP* (2014), p. 1724–1734.
- [4] CLEVERT, D.-A., UNTERTHINER, T., AND HOCHREITER, S. Fast and accurate deep network learning by exponential linear units (elus). In *Preceedings of ICLR* (2016).
- [5] ELFWING, S., UCHIBE, E., AND DOYA, K. Sigmoid-weighted linear units for neural network function approximation in reinforcement learning. *Neural Networks 107* (2018), 3–11. Special issue on deep reinforcement learning.
- [6] FLUSSER, J., FAROKHI, S., HÖSCHL, C., SUK, T., ZITOVÁ, B., AND PEDONE, M. Recognition of images degraded by gaussian blur. *IEEE Transactions on Image Processing 25*, 2 (2016), 790–806.
- [7] HAHNLOSER, R. H., SARPESHKAR, R., MAHOWALD, M. A., DOUGLAS, R. J., AND SEUNG, H. S. Digital selection and analogue amplification coexist in a cortex-inspired silicon circuit. *Nature 405*, 6789 (2000), 947–951.
- [8] HE, K., ZHANG, X., REN, S., AND SUN, J. Delving deep into rectifiers: Surpassing human-level performance on imagenet classification. In *Proceedings of ICCV* (2015).
- [9] HE, K., ZHANG, X., REN, S., AND SUN, J. Deep residual learning for image recognition. In *Proceedings of CVPR* (2016).
- [10] HOCHREITER, S., AND SCHMIDHUBER, J. Long short-term memory. *Neural Computation 9*, 8 (1997), 1735–1780.
- [11] IOFFE, S., AND SZEGEDY, C. Batch normalization: Accelerating deep network training by reducing internal covariate shift. In *Proceedings of ICML* (2015), vol. 37, pp. 448–456.
- [12] KRIZHEVSKY, A. Learning multiple layers of features from tiny images. *Master’s thesis, University of Toronto* (2009).
- [13] KRIZHEVSKY, A., SUTSKEVER, I., AND HINTON, G. E. Imagenet classification with deep convolutional neural networks. *Commun. ACM 60*, 6 (may 2017), 84–90.
- [14] LABATIE, A., MASTERS, D., EATON-ROSEN, Z., AND LUSCHI, C. Proxy-normalizing activations to match batch normalization while removing batch dependence. In *Proceedings of NeurIPS* (2021), vol. 34, pp. 16990–17006.
- [15] LE, T., CHARTRAND, R., AND ASAKI, T. J. A variational approach to reconstructing images corrupted by poisson noise. *Journal of mathematical imaging and vision 27* (2007), 257–263.
- [16] LEE, C.-Y., XIE, S., GALLAGHER, P., ZHANG, Z., AND TU, Z. Deeply-supervised nets. In *Proceedings of AISTATS* (2015), vol. 38, pp. 562–570.
- [17] LUBANA, E. S., DICK, R., AND TANAKA, H. Beyond batchnorm: Towards a unified understanding of normalization in deep learning. In *Proceedings of NeurIPS* (2021), vol. 34, Curran Associates, Inc., pp. 4778–4791.
- [18] MAAS, A. L., HANNUN, A. Y., NG, A. Y., ET AL. Rectifier nonlinearities improve neural network acoustic models. In *Proceedings of ICML* (2013), vol. 30, p. 3.
- [19] MISRA, D. Mish: A self regularized non-monotonic activation function. *arXiv:1908.08681* (2020).
- [20] NAIR, V., AND HINTON, G. E. Rectified linear units improve restricted boltzmann machines. In *Proceedings of ICML* (2010).
- [21] PASZKE, A., GROSS, S., MASSA, F., LERER, A., BRADBURY, J., CHANAN, G., KILLEEN, T., LIN, Z., GIMELSHEIN, N., ANTIGA, L., DESMAISON, A., KOPF, A., YANG, E., DEVITO, Z., RAISON, M., TEJANI, A., CHILAMKURTHY, S., STEINER, B., FANG, L., BAI, J., AND CHINTALA, S. Pytorch: An imperative style, high-performance deep learning library. In *Proceedings of NeurIPS* (2019), vol. 32.

- [22] QIU, S., XU, X., AND CAI, B. Frelu: Flexible rectified linear units for improving convolutional neural networks. In *Proceedings of ICPR (2018)*, pp. 1223–1228.
- [23] RAMACHANDRAN, P., ZOPH, B., AND LE, Q. V. Searching for activation functions. In *Proceedings of ICLR workshop (2018)*.
- [24] RUSSAKOVSKY, O., DENG, J., SU, H., KRAUSE, J., SATHEESH, S., MA, S., HUANG, Z., KARPATY, A., KHOSLA, A., BERNSTEIN, M., ET AL. Imagenet large scale visual recognition challenge. *International journal of computer vision* 115, 3 (2015), 211–252.
- [25] VIJAYKUMAR, V., VANATHI, P., AND KANAGASABAPATHY, P. Fast and efficient algorithm to remove gaussian noise in digital images. *IAENG International Journal of Computer Science* 37, 1 (2010), 300–302.
- [26] XU, B., HUANG, R., AND LI, M. Revise saturated activation functions. *arXiv:1602.05980* (2016).

A Definition of zero-like mean activation

The activation output of the i^{th} unit of m^{th} sample ($m \in \{1, 2, \dots, M\}$) is defined as $a_{i,m} = f(y_{i,m})$, where f , $y_{i,m}$, and M are activation function, the i^{th} activation input of the m^{th} sample, and the number of samples, respectively. Ideally, a “zero-like activation mean” occurs when the activation mean of a single unit, a_i , approximates zero across the samples. Mathematically, this can be represented as:

$$\frac{1}{M} \sum_{m=1}^M a_{i,m} \approx 0.$$

However, approximating the activation mean to zero is challenging for the activation functions that saturate the (large) negative outputs such as ELU, SiLU or FReLU. Due to the saturation, previous studies have defined the “zero-like activation mean” property of an activation function as its ability to “push” the activation mean towards zero. In a mathematical term, this can be presents as $|\mu_{a_i}| \ll c$, where c is a small positive constant [4, 22].

B Difference between LayerAct and activation with LayerNorm

In this section, we compare the activation outputs between LayerAct and activation functions paired with LayerNorm. When LayerNorm is placed right before activation, the output is $a_i = n_i^{LN} s(n_i^{LN})$, where n_i^{LN} is normalized output of LayerNorm. Conversely, the activation output of a LayerAct function is $a_i = y_i s(n_i)$, as defined in Equation 6 in the main article.

The critical distinction between activation with LayerNorm and LayerAct lies in the preservation of input mean and variance statistical information in the activation output. With LayerNorm, the activation function takes a layer-normalized input, resulting in activation outputs that exhibit similar statistical information across samples (as shown in the activation output equation for LayerNorm above). However, this homogenization of statistical information across samples, a characteristic of LayerNorm, is a reason why BatchNorm often outperforms LayerNorm in non-sequential models such as CNNs [14, 17].

LayerAct, on the other hand, preduces more distinguishable activation outputs between samples by preserving statistical variation between samples. This is due to the fact that only the activation scale function of LayerAct uses the layer-normalized input, not the LayerAct function itself (as shown in Equation 6 in the main article).

We would like to note that LayerAct is compatible with BatchNorm, and all the networks used in our CIFAR10, CIFAR100 and ImageNet experiments contain BatchNorm. It is worth noting that the dimension of input normalization between BatchNorm and the activation scale of LayerAct differs, which can result in different effects from BatchNorm to LayerAct. Thus, LayerAct can be effectively used with BatchNorm to enhance the performance of neural networks.

C RNN-based networks with LayerAct

In the networks where activation and LayerNorm have one-to-one correspondence (i.e. LayerNorm is placed right before the activation), the activation input would be the output of LayerNorm:

$$n_i^{LN} = LN(y_i) = g_i \frac{y_i - \mu}{\sqrt{\sigma_y^2 + \alpha}} + b_i,$$

where LN denotes LayerNorm, and n_i^{LN} , g_i and b_i are layer-normalized output, the gain and bias parameters of LayerNorm, respectively. Since n_i^{LN} is already layer-normalized, the activation outputs of element-level activation function, $n_i^{LN} s(n_i^{LN})$, and LayerAct function, $n_i^{LN} s(n_i)$, become more similar when the gain and bias parameters of LayerNorm are closer to zero and one, respectively.

However, there are RNN-based networks without one-to-one correspondence between activation and normalization. An example of this is the LSTM-based network with LayerNorm that proposed by Ba

et al. [1]:

$$\begin{pmatrix} f_t \\ i_t \\ o_t, \\ g_t \end{pmatrix} = LN(W_h h_{t-1}; \alpha_1, \beta_1) + LN(W_x x_t; \alpha_2, \beta_2)$$

$$c_t = \sigma(f_t) \odot c_{t-1} + \sigma(i_t) \odot \tanh(g_t)$$

$$h_t = \sigma(o_t) \odot \tanh(LN(c_t; \alpha_3, \beta_3))$$

where LN and σ denotes LayerNorm and Sigmoid as activation function. In this network, the activation input f , i , and o of σ are the sum of the two layer-normalized outputs and a bias b . This means that the input of the activation scale function, the sum of two layer-normalized outputs from the LayerNorm layer, will differ between LayerAct and element-level activation, leading to different activation outputs. Despite LayerAct and LayerNorm having the same normalization direction, LayerAct functions can still be utilized with LayerNorm in such networks.

D Activation output of LayerAct functions

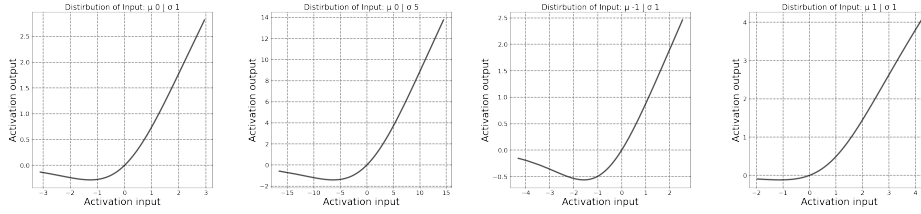


Figure 5: LA-SiLU with different mean and variance value in the input. The distribution of the activation input is: i) $\mu_y = 0, \sigma_y = 1$, ii) $\mu_y = 0, \sigma_y = 5$, iii) $\mu_y = -5, \sigma_y = 1$, and iv) $\mu_y = 5, \sigma_y = 1$ from the left to right.

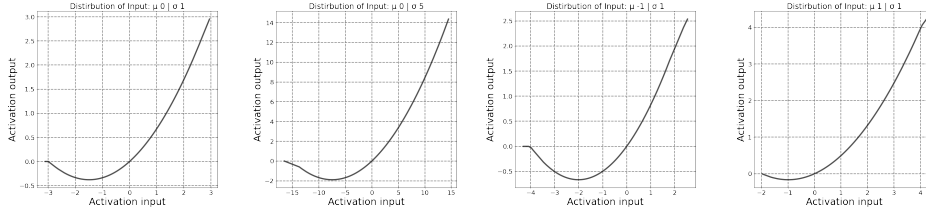


Figure 6: LA-HardSiLU with different mean and variance values in the input. The distribution of the activation input is: i) $\mu_y = 0, \sigma_y = 1$, ii) $\mu_y = 0, \sigma_y = 5$, iii) $\mu_y = -5, \sigma_y = 1$, and iv) $\mu_y = 5, \sigma_y = 1$ from the left to right.

In this section, we present and discuss an illustration of LayerAct functions. Unlike other activation functions, the mean and variance of the input affect the shape of the activation output in the LayerAct functions (as outlined in Equation 6 in the main article). For better demonstration of this characteristic, we present the outputs of the LayerAct functions for four distinct cases. Each cases uses an input that follows a different normal distribution.

Figures 5 and 6 plot the activation outputs of LA-SiLU and LA-HardSiLU, respectively. These figures demonstrate how the shape of activation output are different depending on the shape, mean and variance in this cases, of the activation input. The figures also show that LayerAct functions can produce negative outputs depending on the mean and variance of the inputs. In some cases, no output exists in the saturation state (see the second figure in Figure 6). It is notable that the LayerAct functions achieved noise-robustness without a large number of elements in the saturation state.

E Experimental reproduction

We implemented LayerAct functions and networks for experiment with PyTorch [21]. All networks used in our experiments were trained on NVIDIA A100. We used multiple devices to train the networks on ImageNet, and a single device for the other experiments. The versions of Python and the packages were i) Python 3.9.12, ii) numpy 1.19.5 iii) PyTorch 1.11.0, and iv) torchvision 0.12.0. We used cross entropy loss functions for all the experiments. The random seeds of the experiments were $11 \times i$ where $i \in \{1, 2, \dots, 30\}$ on CIFAR10 and CIFAR100 and 11 and 22 on ImageNet.

To train networks on MNIST for experimental analysis, we applied batch gradient descent for 80 epochs with the weight decay and momentum fixed to 0.0001 and 0.9, respectively. The learning rate started from 0.01, and was multiplied 0.1 at epochs 40 and 60 as scheduled.

We used ResNet [9] with BatchNorm right before activation for experiments on CIFAR10, CIFAR100 and ImageNet. We initialized the weights following the methods proposed by He et al. [8]. For all experiments, the weight decay, momentum, and initial learning rate were 0.0001, 0.9 and 0.1, respectively.

For CIFAR10 and CIFAR100, we trained ResNet20, ResNet32, and ResNet44 with a basic block using the stochastic gradient descent with a batch size of 128 for about 64000 iterations. We randomly selected 10% of the training dataset as the validation set. The learning rate was scheduled to decrease by the factor of 10 at 32000 and 48000 iterations. For the data augmentation of CIFAR10 and CIFAR100, we followed Lee et al. [16]. We rescaled the data between 0 and 1, padded 4 pixels on each side, and randomly sampled a 32×32 crop from the padded image or its horizontal flip. The data was normalized after augmentation. For testing, we did not apply data augmentation, only normalized the data. The hyper-parameter α of LayerAct functions for the experiments was set to 0.00001.

For the experiment with ImageNet, we trained ResNet50 with the bottleneck block using stochastic gradient descent, and the batch size was 256 for about 600000 iterations. The learning rate was scheduled to decrease by a factor of 10 at 180000, 360000, and 540000 iterations. For the data augmentation on ImageNet, we rescaled the data between 0 and 1, resized it to 224×224 , and randomly sampled a 224×224 crop from an image or its horizontal flip [13]. We normalized the data after data augmentation. For testing, we resized the data to be 256×256 and applied 10-crop. Afterward, the data was normalized. To ensure stable learning, we set the hyper-parameter α of LayerAct functions to 0.1 which is larger than those for CIFAR10 and CIFAR100.

The noisy datasets were generated by adding noise to the data after it was rescaled between 0 and 1. Following this, the same data augmentation applied to the clean dataset were also used on the noisy dataset.

F Supplementary material

The supplementary material of this paper and the trained networks are available in our anonymous GitHub repository¹.

¹<https://github.com/LayerAct/LayerAct>

G Additional figures and tables

In this section, we present additional tables and figures extracted from the experiments.

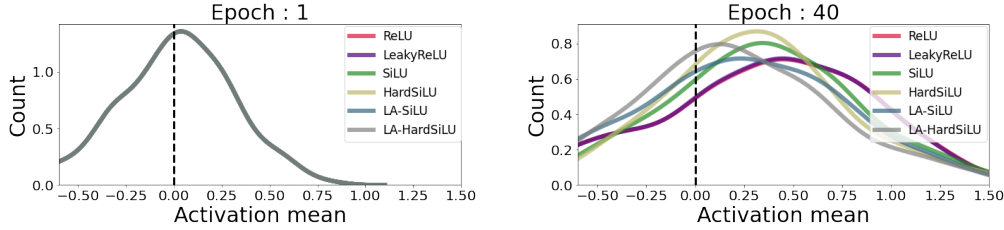


Figure 7: Distribution of the activation **input** means of the elements in a trained network on MNIST at 1st and 40th epochs.

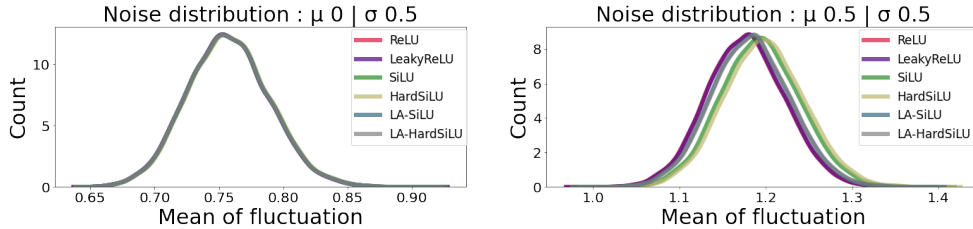


Figure 8: Distribution of activation **input** fluctuation due to noise with different noise distribution.

Figure 7 presents the distribution of the mean activation input. As observed in the mean of activation input at epoch 40 (right), LayerAct functions promote the training of parameter W such that the output of the linear projection $y = W^T x$, which is also activation input, gets closer to zero compared to other functions. This helps the activation output to exhibit a ‘zero-like’ behaviour.

LayerAct functions exhibit a significantly lower mean and variance of activation fluctuation among the samples compared to any other element-level activation function (see Figure 3 in the main article). Figure 8 demonstrates that the distribution of mean fluctuation in activation input appears similar across all functions. This observation confirms that the lower mean and variance of activation output fluctuation of LayerAct functions is not due to a smaller fluctuation in activation input, but is a result of the inherent mechanism of LayerAct.

Table 5: Standard deviation of classification performance on the clean CIFAR10 and CIFAR100.

	CIFAR10			CIFAR100		
	ResNet20	ResNet32	ResNet44	ResNet20	ResNet32	ResNet44
ReLU	0.22	0.39	0.64	0.30	0.53	0.57
LReLU	0.27	0.34	0.45	0.33	0.34	0.70
PReLU	0.24	0.28	-	0.45	0.51	0.72
Mish	0.23	0.25	0.45	0.33	0.49	0.52
SiLU	0.21	0.22	0.25	0.42	0.51	0.53
HardSiLU	0.23	0.22	0.43	0.40	0.54	0.96
LA-SiLU	<u>0.17</u>	<u>0.19</u>	0.28	0.36	<u>0.38</u>	<u>0.44</u>
LA-HardSiLU	0.21	0.31	<u>0.21</u>	0.41	0.46	0.81

Table 5 demonstrate the standard deviation of classification performance on the clean CIFAR10 and CIFAR100 datasets. The lowest results are underlined and bolded, while the second lowest are bolded. The performance of networks with LA-SiLU were similar or more stable compared to other activation functions in most cases.

Table 6: Statistical significance test of LA-SiLU on CIFAR10 dataset.

	CIFAR10					
	ReLU	LReLU	PReLU	Mish	SiLU	HardSiLU
ResNet20	<0.05	<0.05	<0.05	<0.05	<0.05	<0.05
ResNet32	<0.05	<0.05	<0.05	>0.05	>0.05	<0.05
ResNet44	<0.05	<0.05	<0.05	>0.05	<0.05	<0.05

Table 7: Statistical significance test of LA-SiLU on CIFAR100 dataset.

	CIFAR100					
	ReLU	LReLU	PReLU	Mish	SiLU	HardSiLU
ResNet20	<0.05	<0.05	<0.05	<0.05	<0.05	<0.05
ResNet32	<0.05	<0.05	<0.05	<0.05	<0.05	<0.05
ResNet44	>0.05	>0.05	<0.05	>0.05	<0.05	<0.05

Tables 6 and 7 present the results of a statistical significance test between the accuracy of networks with element-level activation functions and those with LA-SiLU on clean CIFAR10 and CIFAR100. When the accuracies of both functions were normally distributed, we performed a T-test. In cases where at least one of them are not, we performed a Wilcoxon signed-rank test otherwise. The notation '>0.05' indicates that the p -value from either a T-test or a Wilcoxon signed-rank test is larger than the standard significance level of 0.05 (i.e. p -value > 0.05). This suggests that LA-SiLU is not significantly better or worse than the alternative function. Conversely, '<0.05' denotes that the p -value is smaller than 0.05, indicating that LA-SiLU is significantly superior to the alternative function (i.e. p -value < 0.05).

Tables 8, 9, 10, and 11 demonstrate the classification performance of ResNet20 and ResNet32 with activation functions on noisy CIFAR10 and CIFAR100 datasets. Six different noisy cases are presented in the tables: i) Gaussian distributed noise with mean and standard deviation as 0 and 0.05, ii) 0.1 and 0.05, iii) 0 and 0.1, iv) 0.1 and 0.1, v) Poisson distributed noise, and vi) Gaussian blur noise with kernel size and standard deviation as (3, 3) and 1. The performance of networks with LayerAct functions were better than other activation functions in most cases.

Figures 9 and 10 display the average accuracy over 30 runs for ResNet20, ResNet32, and ResNet44 on Gaussian noisy CIFAR10 and CIFAR100 with a fixed mean as 0 and different variance. There was no noticeable difference in network performance across different activation functions when the variance of noise was large (Figures 9 and 10). Meanwhile, LayerAct functions were highly performing when noise have large mean. Figures 11 and 12 present the average accuracy over 30 runs for ResNet20, ResNet32, and ResNet44 on Gaussian noisy CIFAR10 and CIFAR100 with different mean and a fixed variance as 0.01^2 , respectively. The robustness of networks with LayerAct functions to the large noise mean is remarkable when compared to those with element-level activation function, especially on CIFAR100 dataset which is more complex than CIFAR10.

In the paper, we reported the classification performance of ResNet50 on ImageNet with random seed 11 for weight initialization. Table 12 demonstrate the experimental result of ResNet50 with activation functions with random seed 22. Network with PReLU exploded during training.

Table 8: Classification performance of ResNet20 on the noisy CIFAR10.

	CIFAR10/ResNet20					
	Gaussian Noise 1	Gaussian Noise 2	Gaussian Noise 3	Gaussian Noise 4	Poisson Noise	Gaussian Blur
ReLU	61.50	60.98	22.33	23.00	75.14	51.10
LReLU	60.72	60.07	22.63	23.25	72.72	51.61
PReLU	60.18	59.35	23.50	23.79	72.48	49.71
Mish	60.17	59.32	22.90	23.31	69.85	51.75
SiLU	61.15	60.27	23.96	24.47	68.64	51.89
HardSiLU	60.17	59.35	22.56	23.16	68.08	52.52
LA-SiLU	63.37	63.14	25.77	26.34	79.91	58.31
LA-HardSiLU	63.29	63.07	26.45	26.79	80.19	58.45

Table 9: Classification performance of ResNet32 on the noisy CIFAR10.

	CIFAR10/ResNet32					
	Gaussian Noise 1	Gaussian Noise 2	Gaussian Noise 3	Gaussian Noise 4	Poisson Noise	Gaussian Blur
ReLU	65.72	65.13	25.37	26.00	74.80	53.44
LReLU	65.57	64.83	25.07	25.65	74.69	54.75
PReLU	65.43	64.66	25.38	25.53	72.56	54.00
Mish	65.30	64.52	26.20	26.49	74.39	53.76
SiLU	64.76	64.06	25.37	25.71	72.26	52.87
HardSiLU	64.62	64.17	24.92	25.74	71.78	53.37
LA-SiLU	66.12	66.09	27.41	28.25	83.56	57.91
LA-HardSiLU	67.44	67.21	30.04	30.67	82.54	58.52

Table 10: Classification performance of ResNet20 on the noisy CIFAR100.

	CIFAR100/ResNet20					
	Gaussian Noise 1	Gaussian Noise 2	Gaussian Noise 3	Gaussian Noise 4	Poisson Noise	Gaussian Blur
ReLU	26.61	26.83	8.57	8.42	23.71	31.50
LReLU	26.95	27.36	8.63	8.80	23.21	31.82
PReLU	24.81	24.59	7.72	7.50	21.26	29.09
Mish	24.94	24.84	7.68	7.51	21.12	30.57
SiLU	26.21	26.17	8.29	8.19	19.78	30.57
HardSiLU	26.19	26.45	8.11	8.12	19.79	30.63
LA-SiLU	27.37	27.62	8.23	8.49	30.80	33.61
LA-HardSiLU	28.62	28.93	8.90	9.12	27.35	34.31

Table 11: Classification performance of ResNet32 on the noisy CIFAR100.

	CIFAR100/ResNet32					
	Gaussian Noise 1	Gaussian Noise 2	Gaussian Noise 3	Gaussian Noise 4	Poisson Noise	Gaussian Blur
ReLU	29.94	29.97	9.85	9.83	22.58	32.20
LReLU	29.51	29.52	9.35	9.24	22.97	32.50
PReLU	29.57	29.25	9.19	8.88	20.76	30.35
Mish	28.29	28.35	8.92	8.75	23.29	31.88
SiLU	29.25	29.29	9.42	9.36	19.93	31.38
HardSiLU	29.90	29.97	9.52	9.47	19.06	31.47
LA-SiLU	31.19	31.86	10.21	10.80	33.62	35.81
LA-HardSiLU	33.18	33.67	11.82	12.49	26.42	36.52

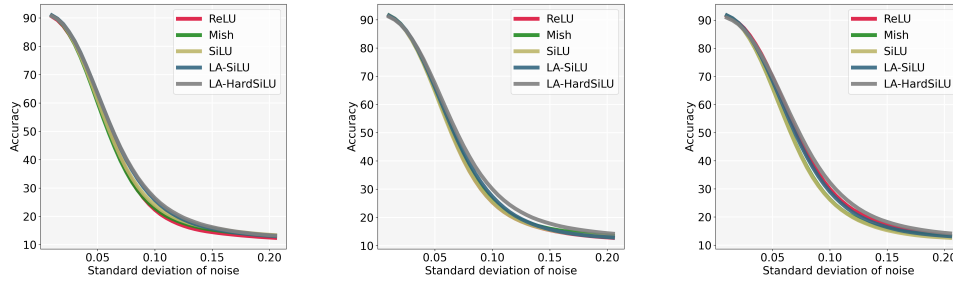


Figure 9: Accuracy plot of ResNet20 (left), ResNet32 (middle), and ResNet44 (right) with activation functions on Gaussian noisy CIFAR10 datasets with fixed mean and different variance.

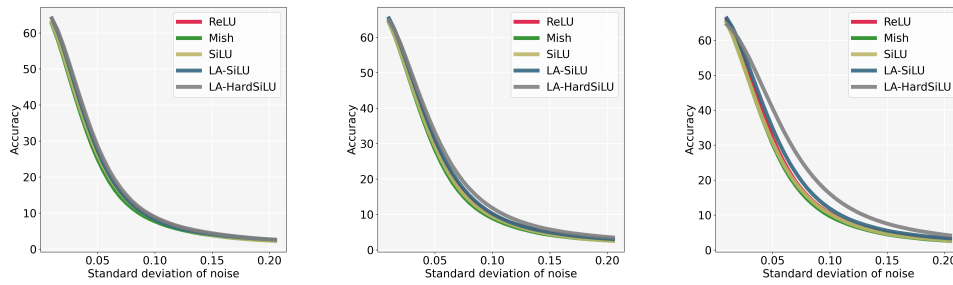


Figure 10: Accuracy plot of ResNet20 (left), ResNet32 (middle), and ResNet44 (right) with activation functions on Gaussian noisy CIFAR100 datasets with fixed mean and different variance.

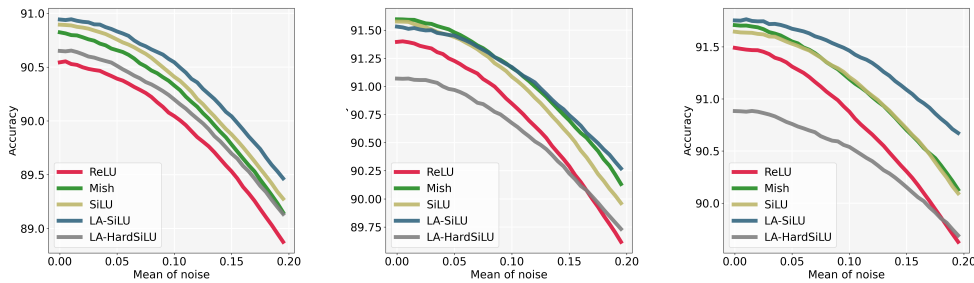


Figure 11: Accuracy plot of ResNet20 (left), ResNet32 (middle), and ResNet44 (right) with activation functions on Gaussian noisy CIFAR10 datasets with different mean and fixed variance.

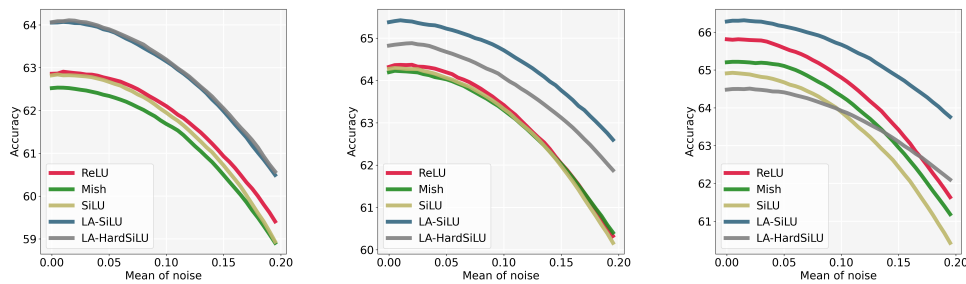


Figure 12: Accuracy plot of ResNet20 (left), ResNet32 (middle), and ResNet44 (right) with activation functions on Gaussian noisy CIFAR100 datasets with different mean and fixed variance.

Table 12: Classification performance on the clean and noisy ImageNet.

	ImageNet/ResNet50				
	Without noise	Gaussian noise 1	Gaussian noise 2	Poisson noise	Gaussian blur
ReLU	78.04	70.15	68.86	8.15	68.79
LReLU	76.86	69.28	68.31	11.26	67.38
Mish	77.66	69.36	67.63	21.34	67.22
SiLU	77.62	69.12	67.67	7.15	67.62
HardSiLU	76.32	67.53	66.00	13.97	64.82
LA-SiLU	78.51	71.85	71.10	49.33	67.08
LA-HardSiLU	78.11	71.67	71.14	38.64	67.37